Focusing characteristics of a 4π parabolic mirror light-matter interface

Lucas Alber,[1,2,*] Martin Fischer,[1,2,*] Marianne Bader,[1,2]
Klaus Mantel,[1] Markus Sondermann,[1,2] and Gerd Leuchs[1,2,3]

[1] *Max Planck Institute for the Science of Light, Guenther-Scharowsky-Str. 1/ building 24, 91058 Erlangen, Germany*[†]
[2] *Friedrich-Alexander-Universität Erlangen-Nürnberg (FAU), Department of Physics, Staudtstr. 7/B2, 91058 Erlangen, Germany*
[3] *Department of Physics, University of Ottawa, Ottawa, Ont. K1N 6N5, Canada*

Focusing with a 4π parabolic mirror allows for concentrating light from nearly the complete solid angle. So far, this idea could not be exploited to enable diffraction limited focusing from more than half solid angle. We present the focusing properties of a 4π parabolic mirror experimentally characterized with a single $^{174}Yb^{+}$ ion as a mobile point scatterer. The ion is trapped in a vacuum environment with a movable high optical access Paul trap. We demonstrate an effective focal spot size of 209 nm in lateral and 551 nm in axial direction. Such tight focusing allows us to build an efficient light-matter interface. Our findings agree with numerical simulations incorporating a finite ion temperature and interferometrically measured wavefront aberrations induced by the parabolic mirror. We point at further technological improvements and discuss the general scope of applications of a 4π parabolic mirror.

arXiv:1609.06884v1 [quant-ph] 22 Sep 2016

I. INTRODUCTION

Free space interaction between light and matter is incorporated as a key technology in many fields in modern science. The efficiency of interaction influences measurements and applications ranging from various kinds of fundamental research to industrial applications. New innovations and new types of high precision measurements can be triggered by improving the tools needed for a light-matter interface. To achieve high interaction probability with a focused light field in free space, a new concept has come up in recent years [1–3]. The concept exploits mode matching of the focused radiation to an electric dipole mode (cf. Ref. [4] and citations therein).

Focusing in free-space experiments is usually done with state-of-the-art lens based imaging systems [5–8]. Single lenses, however, suffer from inherent drawbacks like dispersion induced chromatic aberrations, optical aberrations, and auto-fluorescence, respectively. Most of these limitations can be corrected to a high degree by precisely assembling several coated lenses in a lens-system, *e.g.* in a high numerical aperture (NA) objective. Although solving some problems, multi-lens-systems induce new problems such as short working distances, low transmission for parts of the optical spectrum, the need for immersion fluids, and high costs, respectively. Therefore, multi-lens systems are often application specific providing best performance only for the demands that are most important for the application.

Mirror based objectives are an alternative to lens-based systems and can overcome some of these problems. The improvement is based on a mirror's inherent property of being free from chromatic aberrations. The nearly wavelength independent behavior also leads to a homogeneous reflectivity for a large spectral window. Comparing the reflectivity of mirrors to the transmission of lens based objectives, mirrors can sometimes also surpass lens-based systems. But surprisingly, they are rarely used when high interaction efficiency is required. This lack in application may be due to the fact that reflecting imaging systems, like the Cassegrain reflector, cannot provide a high NA. A high NA is however needed for matching the emission pattern of a dipole, which spans over the entire solid angle. The limitation in NA consequently constitutes a limitation in the maximum achievable light-matter coupling efficiency.

High NA parabolic mirrors ($NA = 0.999$) have meanwhile been successfully applied as objectives in confocal microscopy [9, 10], demonstrating the potential for imaging applications. The parabolic mirror (PM) is a single optical element that, in theory, can cover nearly the complete 4π solid angle for tight focusing [11]. In this article we report on the realization of such a 4π parabolic mirror (4π-PM) and characterize its optical performance. The mirror's focusing capabilities are applied in a light-matter interface with a single $^{174}Yb^{+}$ ion, trapped in a stylus like movable Paul trap [12]. In the interface, we move the ion trap to position the ion in the focus of the parabolic mirror and focus light onto it. Thereby, a solid angle of 94 % that is relevant for a linear dipole transition is covered for focusing. This number especially exceeds an experiment we previously reported that was technically limited to 50 % of the solid angle [13]. Based on the large solid angle coverage, tight focusing from all spatial directions is expected. This is proven by measuring the effective excitation point spread function (PSF) of our focusing system. We compare our findings with simulations incorporating a finite ion temperature and interferometrically measured wavefront aberrations of the parabolic mirror itself. In our discussion, the parabolic mirror is compared to other high NA focusing tools, especially to lens-based 4π mi-

* These authors contributed equally to this work.
† lucas.alber@mpl.mpg.de

croscopes. Its possible field of application is discussed and further improvements to the existing set-up are proposed.

II. SETUP AND EXPERIMENT

Our main experimental intention is to focus light to a minimal spot size in all spatial directions simultaneously. The highest electric energy density that can be realized with any focusing optics is created by an electric dipole wave [14]. We therefore choose this type of spatial mode in our experiment. The electric dipole wave is created by first converting a linear polarized Gaussian beam into a radially polarized donut mode via a segmented half-wave plate (B- Halle) [15, 16]. Second, the radially polarized donut mode is focused with a parabolic mirror onto the trapped ion. This, in theory, enables us to convert approximately 91 % of the donut mode into a linear dipole mode [17]. The conversion efficiency is limited since the donut mode is only approximating the ideal spatial mode that is necessary to create a purely linear dipole mode [2, 18] by being focused with the parabolic mirror. The donut mode, however, yields the experimental advantage of being propagation invariant and comparably easy to generate.

Our focusing tool, the parabolic mirror, is made of diamond turned aluminum (Fraunhofer Institute for Applied Optics and Precision Engineering, Jena) with a reflectivity of 64 % for the incident mode at a wavelength of $\lambda_{exc} = 369.5\,\text{nm}$. Its geometry has a focal length of 2.1 mm and an outer aperture of 20 mm in diameter. In total, the geometry covers 81 % of the complete solid angle. This fraction corresponds to 94 % of the solid angle that is relevant for coupling to a linear dipole oriented along the axis of symmetry [11, 17]. Furthermore, the mirror has three bores near its vertex: two bores with a diameter of 0.5 mm for dispensing neutral atoms and for illuminating the ion with additional laser beams, respectively; and one bore with a diameter of 1.5 mm for the ion trap itself. The ion trap is a Stylus-like Paul trap similar to [12] with high optical access. The trap is mounted on a movable xyz piezo translation stage (PIHera P-622K058, Physik Instrumente) that is used for measuring the effective excitation *PSF*. The effective excitation *PSF* is defined as the convolution of the focal intensity distribution with the spatial extent of the ion.

We measure the effective excitation *PSF* by probing the focal spot at different positions. In order to do so, we use the translation stage to scan the ion through the focal spot with an increment of 25 nm. At each position, the incoming dipole mode excites the $S_{1/2}$ - $P_{1/2}$ transition that has a wavelength of $\lambda_{exc} = 369.5\,\text{nm}$. The relevant energy levels of $^{174}Yb^{+}$ are shown in figure 1. We weakly drive this transition such that the probability for exciting the ion into the $P_{1/2}$ state is proportional to the electric energy density at any point in the focal area. During these

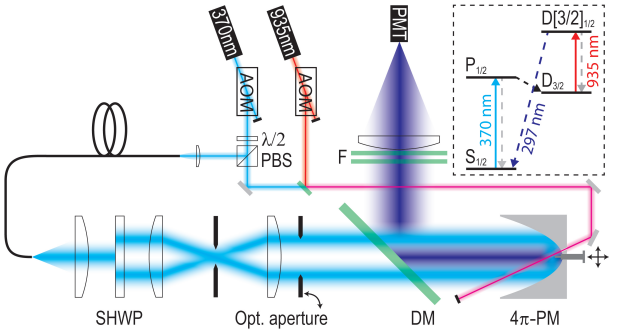

FIG. 1. Optical set-up of the experiment and relevant energy levels of $^{174}Yb^{+}$. The cooling laser (blue) and the repump laser (red) are focused onto the ion through a hole at the backside of the parabolic mirror. AOM - acousto optical modulator, DM - dichroic mirror, F - clean up filter, 4π-PM - 4π parabolic mirror, PMT - photo multiplier tube, SHWP - segmented half-wave plate.

measurements, the ion is Doppler cooled by the focused donut mode. Hence, the detuning of this mode relative to the $S_{1/2}$ - $P_{1/2}$ transition and its power determine the temperature of the ion, see appendix for further details.

Since we excite the ion from nearly the complete solid angle, we cannot directly detect the fluorescent response of the ion at the same wavelength. Instead, we detect photons at a wavelength of $\lambda_{det} = 297.1\,\text{nm}$ allowing us to independently focus and detect from nearly the complete solid angle. Photons at the detection wavelength λ_{det} are emitted during the spontaneous $D[3/2]_{1/2}$ - $S_{1/2}$ decay [19]. The $D[3/2]_{1/2}$ level is populated when the ion spontaneously decays from the excited $P_{1/2}$ state into the metastable $D_{3/2}$ state (0.5% probability, lifetime of 52 ms [20]). From this state, we optically pump the ion into the $D[3/2]_{1/2}$ state by saturating the $D_{3/2}$ - $D[3/2]_{1/2}$ transition with a strong laser field at a wavelength of 935.2 nm (DL-100, Toptica Photonics). This infrared laser is co-aligned with a second laser at the excitation wavelength λ_{exc} (TA-SHG pro, Toptica Photonics) and both are sent through the focus of the parabolic mirror via one of its backside bores (see figure 1). The second laser at the excitation wavelength λ_{exc} is used for ionization.

The emitted fluorescent photons at the detection wavelength λ_{det} are out-coupled from the excitation beam path via a dichroic mirror (FF310-Di01, Semrock) and two clean up-filters (FF01-292/27-25, Semrock). Afterwards, we detect them with a photomultiplier tube in Geiger mode operation (MP-942, Perkin Elmer) that has a remaining underground/dark count rate of 10 - 20 cps. The overall detection efficiency η_{det} at the detection wavelength λ_{det} was measured via pulsed excitation and amounts to $\eta_{det} \approx 1.4\,\%$. The detection efficiency is needed for the determination of the coupling efficiency to the trapped ion. Based on the atomic decay rate on the detected transition, the total fluorescence count rate would be approximately

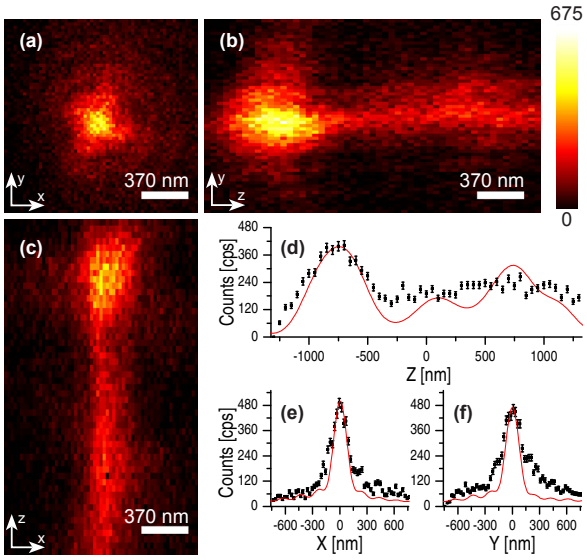

FIG. 2. Effective excitation *PSF* in the xy (a), zy (b), and xz (c) plane when illuminating the *full solid angle* covered by the 4π-PM. The corresponding line profiles through the center of the focus are shown in (d-f). They are overlayed to the line profiles resulting from numerical simulations (red)

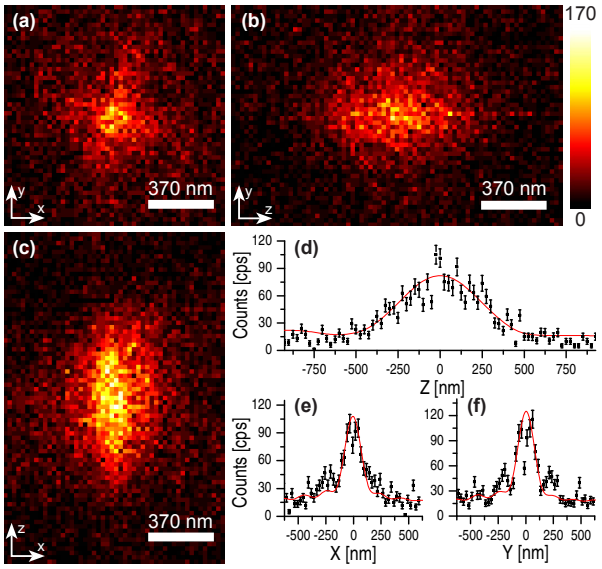

FIG. 3. Effective excitation *PSF* similar to figure 2 but for illuminating *half of the solid angle* of the 4π-PM. This is accomplished by using the optional aperture shown in figure 1.

154 kcps for $S = 1$. Taking into account the finite detection efficiency, we would expect to measure approximately 2160 cps.

The coupling efficiency is measured by recording the detection count rate R_{det} as a function of the excitation power P_{exc}. Analyzing the four-level quantum master equation we find that both quantities are proportional to each other in the limit of strong repumping powers. The dependence of R_{det} for varying excitation power is approximated by

$$R_{det} \approx \eta_{det}\,\beta\,\frac{\Gamma}{2}\frac{S}{S+1}$$

with β denoting the branching ratio from the $P_{1/2}$ state into the $D_{3/2}$ state, Γ the $S_{1/2}$ - $P_{1/2}$ transition linewidth, and S the saturation parameter, respectively. S is defined as $S = GP_{exc}/P_{sat}$ with the coupling efficiency G and the saturation power $P_{sat} = \frac{hc}{\lambda_{exc}}\frac{\Gamma}{8}(1+4(\Delta/\Gamma)^2)$, respectively [13]. Δ is the detuning of the excitation laser from the $S_{1/2}$ - $P_{1/2}$ resonance. The formula for the detection count rate enables us to determine the coupling efficiency by curve fitting of our measured data. During the measurement of the coupling efficiency, we position the ion exactly in the maximum of the excitation *PSF*, *i.e.* we measure the maximum coupling efficiency obtainable in the focal region under the current experimental conditions.

III. RESULTS

The experimental results for the effective excitation *PSF* are shown in figure 2. We measure a spot size of 237 ± 10 nm (*FWHM*) in the lateral direction (a, e, f). In the axial direction (b - d), however, the focal peak is broadened due to optical aberrations. The influence of the aberrations is reduced, when we limit the front aperture of the 4π-PM to half solid angle (figure 3). The reduced aperture results in a lateral width of 209 ± 20 nm and an axial width of 551 ± 27 nm. These values include the influence of the finite spatial extent of the trapped ion (see appendix). In the Doppler limit, this extent is approximately 140 nm in lateral and 80 nm in axial direction considering the trap frequencies $\omega_{\text{lateral}}/2\pi \cong 490$ kHz and $\omega_{\text{axial}}/2\pi \cong 1025$ kHz, respectively, and a detuning from resonance of about 14.1 MHz.

To estimate the contribution of the ion-size to the focal broadening, we simulate the excitation *PSF* based on a generalization of the method presented in [21]. Our calculation also includes the aberrations of the parabolic mirror which were measured interferometrically beforehand [22]. The intensity distributions resulting from these simulations are subsequently convolved with the spatial extent of the ion to achieve the effective excitation *PSF*.

The outcomes of our simulations are shown in table I. The effective *PSF* obtained in the simulations exhibits a good qualitative agreement with the *PSF* obtained in the experiment, cf. figure 2 and 3. Based on these results, the coupling efficiency G is expected (see appendix) to be $G = 8.7\,\%$ for illuminating the full aperture and $G = 14.3\,\%$ for limiting the aperture of the 4π-PM to half solid angle. These values are corrected for the fact that we are not driving a closed two-level transition [13]. From the data shown in figure 4, we measure a coupling efficiency of $G = 8.6 \pm 0.9\,\%$ (full solid angle) and $G = 13.7 \pm 1.4\,\%$ (half solid an-

TABLE I. Influence of experimental factors on the effective excitation *PSF* (eff. exc. *PSF*). The full width at half maximum is given for illuminating full solid angle (FSA) and half solid angle (HSA) of the 4π-PM, respectively. In case of illuminating the full solid angle and considering optical aberrations, no distinct peak can be identified along the axial direction.

Simulation		Lateral		Axial	
		HSA	FSA	HSA	FSA
Exc. *PSF*	ideal mirror (i.m.)	139 nm	142 nm	412 nm	253 nm
	aberrated mirror (a.m.)	135 nm	135 nm	536 nm	
	i.m. with ion-extent	189 nm	192 nm	418 nm	266 nm
	a.m. with ion-extent	189 nm	189 nm	542 nm	
Eff. exc. *PSF* (measurement)		209 ± 20 nm	237 ± 10 nm	551 ± 27 nm	

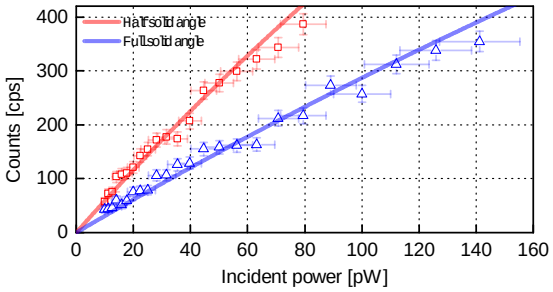

FIG. 4. Saturation measurement of the coupling efficiency and the respective curves from curve fitting (solid lines) when illuminating half of the solid angle (red) and full solid angle (blue). Only data points for weak excitation ($R_{det} \leq 392$ cps) are used for fitting (see appendix).

gle). These values are close to the expected values from the simulations taking into account all current deficiencies of the set-up.

IV. DISCUSSION

Concentration of light into a narrow three dimensional volume is involved in many scientific applications. The scope ranges from applications that require "classical" light fields, like light microscopy, optical traps and material processing, to applications in quantum information science. In quantum information science, tight focusing of light is the key ingredient for free-space light-matter interfaces with a high coupling efficiency. This kind of free-space set-up may be an alternative to cavity based light-matter interfaces also providing high interaction strength. But in contrast to cavity assisted set-ups, free-space experiments often have a low level of instrument complexity and provide higher bandwidth. This is important considering the scalability and flexibility of an experimental set-up.

Technically, concentration of light is done by using focusing optics. How tight the focusing will be, depends on the numerical aperture of the focusing optics that is given by $NA = n \sin(\alpha)$, $NA \in [0, n]$, where α is the half-opening angle of the optics' aperture and n is the refractive index of the surrounding medium. For high NA objectives, the exact dependence of the focal volume as a function of NA can only be calculated numerically incorporating a vectorial treatment of the electric field. But as the numerical aperture increases, the focal volume will basically decrease.

For a 4π focusing optic, the numerical aperture is no longer defined. Nevertheless, it seems obvious that diffraction limited focusing from more than half of the hemisphere would produce a smaller three-dimensional focal volume. Consequently, a different quantity has to be used for comparing the performance of different 4π focusing optics. One suitable quantity is the weighted solid angle $\Omega \in [0, 1]$ (normalized to $8\pi/3$) [17]. It is the solid angle that is covered by the focusing optics weighted by the dipole's angular irradiance pattern. Ω defines the maximum fraction of incident power that can be coupled into the dipole mode of a single emitter. Consequently, it provides information about the ability to concentrate light since an electric dipole mode achieves the highest possible energy concentration [14]. $\Omega = 1$ therefore means, that all of the light is coupled into the dipole mode, assuming the ideal radiation pattern. The focusing capabilities of such a focusing optics can not be exceeded by any other optics. In figure 5, the maximal conversion efficiency into a linear dipole wave Ω_{linear} is compared for different (4π) focusing systems also including the 4π-PM geometry used in the experiment. In case of our 4π-PM, one has $\Omega_{linear} = 0.94$. The same fraction of the weighted solid angle can be covered using two opposing objective lenses each having a NA of 0.997 in vacuum. High quality objectives of such high numerical aperture are, however, not available.

In the experiment, the weighted solid angle covered by the focusing optics is one quantity that determines the measured light-matter coupling efficiency. Other important experimental factors are the optical aberrations and the spatial extent of the ion, respectively. Under ideal conditions, we expect a coupling efficiency of $G = \eta^2 \cdot 94\,\% \approx 91\,\%$ where $\eta \approx 0.98$ is the field overlap with the ideal dipole mode [16]. But in our measurements, we are not able to reach this limit. Our numerical simulations imply, however, that we are currently not primarily limited by the covered solid angle, but by the spatial extent of the ion and the optical

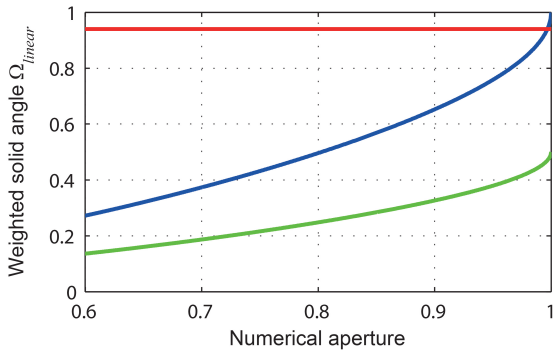

FIG. 5. Weighted solid angle Ω_{linear} covered by a single objective lens (green), by a lens based 4π-microscope (blue), and by the 4π-PM geometry used in the experiment (red).

aberrations (see table I).

Enhancing the optical properties of our focusing system and therefore also the coupling efficiency can be done by correcting for the aberrations. The predominant aberrations in our set-up are due to form deviations of the mirror from the ideal parabolic shape. A higher degree of form accuracy could be provided by including interferometric measurement techniques [22] into the mirror's production process. Alternatively, the aberrations can be corrected by preshaping the incident wavefront before it enters the parabolic mirror. Wavefront shaping techniques may rely on adaptive optical elements (*e.g.* liquid crystal display, deformable mirror) or a (gray tone) phase plate. The latter technique has already been tested for a 4π-PM of the same geometry as used here [16]. Involving a second optical element for wavefront correction in front of the parabolic mirror would only slightly add complexity to the system. If the corrective element is reflection and refraction based, like a continuous membrane deformable mirror is, the wavelength-independent character of the imaging system is retained.

The wavelength-independent character is the reason why the 4π-PM is intrinsically free of chromatic aberrations. This is beneficial for applications that require tight focusing not only for a monochromatic light source. Typical applications can be found in the field of microscopy: Confocal fluorescence microscopy [23] usually requires correction for the excitation and the detection wavelength; RESOLFT-type far-field Nanoscopy [24] in addition requires correction for the depletion beam. Further examples are two- and three-photon microscopy [25, 26] or Raman microscopy [27]. The variety of reflective materials allows to specialize the 4π-PM for a specific application, *e.g.* for high power applications, high sensitivity measurements or even for applications where wavelengths from the deep UV to the far IR are used at the same time. This ability may enable new illumination or imaging techniques that are not possible with today's technology.

V. CONCLUSION

We experimentally characterized a light-matter interface based on a 4π-PM. By limiting its aperture, we could demonstrate an effective excitation *PSF* having a lateral spot size of $209 \pm 20\,\mathrm{nm}$ in vacuum. That corresponds to $0.57 \cdot \lambda_{exc}$. Using the full mirror we observed a strong splitting of the focal peak along the axial direction due to form deviations of the parabolic mirror. Measuring the induced aberrations interferometrically and including the results in numerical simulations yields values that are consistent with the experiment. In addition, we measured the light-matter coupling efficiency to be $G = 13.7 \pm 1.4\,\%$. This value is also in good agreement with our simulations. Our findings allow us to infer that we are currently limited by the aberrations of the parabolic mirror and the spatial extent of the ion.

We can surpass our current technical limitations by correcting the aberrations of the 4π-PM. This would even further reduce the focal spot size and increase the coupling efficiency. Ways for wavefront correction were given in the discussion section of this work. We also may apply higher trap frequencies or ground state cooling techniques to reduce the spatial extent of the ion. Alternatively, we can trap doubly ionized Ytterbium in our experimental set-up [28]. When trapping a $^{174}Yb^{2+}$ ion we may not need to change the trapping or cooling techniques because the ion's spatial extent is smaller in the Doppler limit (higher charge, narrower transition linewidth). Furthermore, $^{174}Yb^{2+}$ provides a closed two-level transition that is desirable in many experiments on the fundamentals of light-matter interaction. This may be a path for realizing a set-up capable of reaching the ultimate limitations of focusing in free space [2, 11].

ACKNOWLEDGEMENTS

The authors thank S. Heugel, B. Srivathsan, I. Harder and M. Weber for fruitful discussions and M. Weber for valuable comments on the manuscript. G.L. acknowledges financial support from the European Research Council via the Advanced Grant 'PACART'.

VI. APPENDIX

We simulate the focal intensity distribution along the principal axes of our system (x, y, z) based on a generalization of the method presented in [21] including the aberrations of our parabolic mirror. The resulting intensity distributions are convolved with the spatial extent of the ion along the corresponding trap axis. Thus we obtain the motionally induced reduction of the average intensity of the light interacting with the ion for each spatial direction individually. The values obtained for each direction are multiplied. The same procedure is repeated for an aberration-free

parabolic mirror and a point-like ion. Division of these two values and multiplication of the result with the field overlap $\eta^2 \approx 0.982^2$ [16, 17] of the donut mode yields the expected coupling efficiency.

For determining the spatial extent of the Doppler cooled ion, we assume it to be in a thermal state [29]. Hence the spatial extent in each dimension is described by a Gaussian shaped wave packet with width σ_i, $i \in (x, y, z)$. The width can by calculated from the ground state wave packet $\sigma_{i,0}$ by [29]

$$\sigma_i = \sqrt{2\overline{n}_i + 1}\,\sigma_{i,0},$$

where $\overline{n}_i$ denotes the mean phonon number of the harmonic oscillator in i-th direction . The probability $\rho_i(x_i)$ for finding the ion at x_i is described by

$$\rho_i(x_i) = \frac{1}{\sigma_i\sqrt{2\pi}} e^{-\frac{1}{2}(\frac{x_i}{\sigma_i})^2}.$$

In the limit of weak excitation and for the detuning from resonance present in the experiment ($\Delta = 14.2\,\mathrm{MHz}$), the mean phonon numbers are calculated using the rate equations from [30]. For the geometry of our laser beam and trap geometry they amount to $\overline{n}_x = 28.5$, $\overline{n}_y = 27.9$, and $\overline{n}_z = 21.7$, respectively. The trap frequencies are determined by applying an AC signal to one of the compensation electrodes and scanning the applied frequency over the frequency range supposed to contain the trap frequencies while monitoring the the rate of fluorescence photons. We find the trap frequencies $\omega_x/2\pi = 482.6\,\mathrm{kHz}$, $\omega_y/2\pi = 491.7\,\mathrm{kHz}$, and $\omega_z/2\pi = 1025\,\mathrm{kHz}$, respectively.

We only use excitation powers P_{exc} such that $S \leq 1/10$. This equals a detection count rate of $R_{det} \leq 392\,cps$. For larger excitation powers, we expect the spatial extent of the ion to be comparable to the size of the focal intensity distribution. Since $\overline{n} \propto \sqrt{1+S}$ keeping $S \leq 0.1$ ensures that the spatial extent of the ion is approximately constant over the whole measurement range.

[1] S. Quabis, R. Dorn, M. Eberler, O. Glöckl, and G. Leuchs, Optics Communications **179**, 1 (2000).

[2] M. Sondermann, R. Maiwald, H. Konermann, N. Lindlein, U. Peschel, and G. Leuchs, Applied Physics B **89**, 489 (2007).

[3] M. Stobińska, G. Alber, and G. Leuchs, EPL (Europhysics Letters) **86**, 14007 (2009).

[4] G. Leuchs and M. Sondermann, Journal of Modern Optics **60**, 36 (2013), http://dx.doi.org/10.1080/09500340.2012.716461.

[5] N. Piro, F. Rohde, C. Schuck, M. Almendros, J. Huwer, J. Ghosh, A. Haase, M. Hennrich, F. Dubin, and J. Eschner, Nat Phys **7**, 17 (2011).

[6] M. K. Tey, G. Maslennikov, T. C. H. Liew, S. A. Aljunid, F. Huber, B. Chng, Z. Chen, V. Scarani, and C. Kurtsiefer, New Journal of Physics **11**, 043011 (2009).

[7] G. Wrigge, I. Gerhardt, J. Hwang, G. Zumofen, and V. Sandoghdar, Nat Phys **4**, 60 (2008).

[8] D. Pinotsi and A. Imamoglu, Phys. Rev. Lett. **100**, 093603 (2008).

[9] A. Drechsler, M. Lieb, C. Debus, A. Meixner, and G. Tarrach, Opt. Express **9**, 637 (2001).

[10] J. Stadler, C. Stanciu, C. Stupperich, and A. J. Meixner, Opt. Lett. **33**, 681 (2008).

[11] N. Lindlein, R. Maiwald, H. Konermann, M. Sondermann, U. Peschel, and G. Leuchs, Laser Physics **17**, 927 (2007).

[12] R. Maiwald, D. Leibfried, J. Britton, J. C. Bergquist, G. Leuchs, and D. J. Wineland, Nature Physics **5**, 551 (2009).

[13] M. Fischer, M. Bader, R. Maiwald, A. Golla, M. Sondermann, and G. Leuchs, Applied Physics B **117**, 797 (2014).

[14] I. M. Bassett, Optica Acta: International Journal of Optics **33**, 279 (1986).

[15] S. Quabis, R. Dorn, and G. Leuchs, Applied Physics B **81**, 597 (2005).

[16] A. Golla, B. Chalopin, M. Bader, I. Harder, K. Mantel, R. Maiwald, N. Lindlein, M. Sondermann, and G. Leuchs, Eur. Phys. J. D **66**, 190 (2012), arXiv:1207.3215.

[17] M. Sondermann, N. Lindlein, and G. Leuchs, ArXiv e-prints (2008), arXiv:0811.2098 [physics.optics].

[18] G. Alber, J. Z. Bernád, M. Stobińska, L. L. Sánchez-Soto, and G. Leuchs, Phys. Rev. A **88**, 023825 (2013).

[19] H. M. Meyer, M. Steiner, L. Ratschbacher, C. Zipkes, and M. Köhl, Physical Review A **85**, 012502 (2012).

[20] S. Olmschenk, K. C. Younge, D. L. Moehring, D. N. Matsukevich, P. Maunz, and C. Monroe, Physical Review A **76**, 052314 (2007).

[21] B. Richards and E. Wolf, Proceedings of the Royal Society of London A: Mathematical, Physical and Engineering Sciences **253**, 358 (1959).

[22] G. Leuchs, K. Mantel, A. Berger, H. Konermann, M. Sondermann, U. Peschel, N. Lindlein, and J. Schwider, Applied Optics **47**, 5570 (2008).

[23] C. J. R. Sheppard and A. Choudhury, Optica Acta: International Journal of Optics **24**, 1051 (1977).

[24] S. W. Hell, Science **316**, 1153 (2007).

[25] N. G. Horton, K. Wang, D. Kobat, C. G. Clark, F. W. Wise, C. B. Schaffer, and C. Xu, Nature Photonics **7**, 205 (2013).

[26] W. Denk, J. H. Strickler, and W. W. Webb, Science **248**, 73 (1990).

[27] M. E. Andersen and R. Z. Muggli, Analytical Chemistry **53**, 1772 (1981), http://dx.doi.org/10.1021/ac00235a013.

[28] S. Heugel, M. Fischer, V. Elman, R. Maiwald, M. Sondermann, and G. Leuchs, Journal of Physics B: Atomic, Molecular and Optical Physics **49**, 015002 (2016).

[29] J. Eschner, The European Physical Journal D **22**, 341 (2003).

[30] J. Eschner, G. Morigi, F. Schmidt-Kaler, and R. Blatt, J. Opt. Soc. Am. B **20**, 1003 (2003).